PHILOSOPHICAL TRANSACTIONS OF THE ROYAL SOCIETY A MATHEMATICAL, PHYSICAL & ENGINEERING SCIENCES

Anisotropic nuclear spin interactions in $H_2O@C_{60}$ determined by solid-state NMR

M. Concistrè, S. Mamone, M. Denning, G. Pileio, X. Lei, Y. Li, M. Carravetta, N. J. Turro and M. H. Levitt

Phil. Trans. R. Soc. A 2013 **371**, 20120102, published 5 August 2013

PHILOSOPHICAL TRANSACTIONS OF THE ROYAL SOCIETY A

rsta.royalsocietypublishing.org

Research

Cite this article: Concistrè M, Mamone S, Denning M, Pileio G, Lei X, Li Y, Carravetta M, Turro NJ, Levitt MH. 2013 Anisotropic nuclear spin interactions in $H_2O@C_{60}$ determined by solid-state NMR. Phil Trans R Soc A 371: 20120102.
http://dx.doi.org/10.1098/rsta.2012.0102

One contribution of 13 to a Theo Murphy Meeting Issue 'Nanolaboratories: physics and chemistry of small-molecule endofullerenes'.

Subject Areas:
spectroscopy

Keywords:
solid-state NMR, endohedral water fullerene, spin interaction

Author for correspondence:
M. Concistrè
e-mail: mariac@soton.ac.uk

†Deceased 24 November 2012.

Royal Society Publishing
Informing the science of the future

Anisotropic nuclear spin interactions in $H_2O@C_{60}$ determined by solid-state NMR

M. Concistrè[1], S. Mamone[1], M. Denning[1], G. Pileio[1], X. Lei[2], Y. Li[2], M. Carravetta[1], N. J. Turro[2,†] and M. H. Levitt[1]

[1]School of Chemistry, University of Southampton, Highfield, Southampton SO17 1BJ, UK
[2]Department of Chemistry, Columbia University, 3000 Broadway, New York, NY 10027, USA

We report a solid-state NMR study of the anisotropic nuclear spin interactions in $H_2O@C_{60}$ at room temperature. We find evidence of significant dipole–dipole interactions between the water protons, and also a proton chemical shift anisotropy (CSA) interaction. The principal axes of these interaction tensors are found to be perpendicular. The magnitude of the CSA is too large to be explained by a model in which the water molecules are partially aligned with respect to an external axis. The evidence indicates that the observed CSA is caused by a distortion of the geometry or electronic structure of the fullerene cages, in response to the presence of the endohedral water.

1. Introduction

Closed fullerene cages encapsulating small molecules are stable substances that can be synthesized via molecular surgery [1–3]. These extraordinary compounds, available in macroscopic quantities, offer the almost unique possibility to study molecules in a well-insulated, well-defined and highly symmetric environment. The guest molecules encapsulated in these endohedral fullerenes behave as quantum rotors, whose rotational and translational levels are mixed together by the confinement provided by the cage, strongly influencing their spectroscopic properties. Studies of this kind have already been performed on samples of $H_2@C_{60}$, $HD@C_{60}$ and $H_2O@C_{60}$, which have been investigated by far-infrared spectroscopy, inelastic neutron scattering and nuclear magnetic resonance (NMR) [4–13].

The endohedral water fullerene $H_2O@C_{60}$ is a particularly interesting system since water exhibits *ortho–para* spin isomerism and also a strong electric dipole moment. The C_{60} cage provides an environment of icosahedral symmetry, which is expected to lead to a triply degenerate *ortho*-H_2O ground state. Nevertheless, physical studies by a range of techniques, including infrared spectroscopy, inelastic neutron scattering and cryogenic NMR have shown that the degeneracy of the *ortho*-H_2O ground state is lifted in $H_2O@C_{60}$ [4]. This implies a reduction in symmetry, which could be due to partial orientation of the water electric dipoles by a local electric field, or to distortion of the geometry or electronic distribution in the fullerene cage, or to a combination of these effects.

The broken symmetry of the water environment in $H_2O@C_{60}$ leads to a residual dipolar coupling between the water protons, which gives rise to dipole-induced spinning sidebands in cryogenic magic-angle-spinning (MAS) NMR spectra [4]. The sideband pattern of the MAS NMR spectrum at 20 K is consistent with randomly oriented proton pairs coupled by a dipole–dipole magnetic interaction of −5.5 kHz [4]. The residual dipole–dipole coupling interaction may be interpreted in terms of a splitting in the *ortho*-H_2O ground state by an energy of about 0.5 meV, which matches observations by inelastic neutron scattering [4].

The question arises as to whether this symmetry-breaking effect is specific to the cryogenic regime, or whether it arises also at high temperature. In this paper, we describe MAS NMR spectra taken at room temperature, which show clear evidence of nuclear anisotropic spin interactions in $H_2O@C_{60}$. In order to investigate the source of these spinning sidebands, we estimated the residual dipolar coupling between the water protons using a double-quantum-filtered dipolar recoupling (DQfDR) technique [14]. We show that the residual dipole–dipole coupling coexists with a chemical shift anisotropy (CSA) interaction. The magnitude of the observed CSA is inconsistent with partial orientation of the water molecules, and is attributed to distortion or polarization of the enclosing cage.

2. Material and methods

(a) Sample

The sample of $H_2O@C_{60}$ (figure 1*a*) was synthesized according to the method of Kurotobi & Murata [3]. The solution NMR spectrum of the last intermediate prior to cage closure indicated that about 60% of the C_{60} cages are occupied by water molecules.

The sample was purified in two stages. In the first stage (p1), the sample was purified by column chromatography, eluted with CS_2/pentane = 2/1 and dissolved in CS_2. A precipitate was formed by adding pentane. The precipitate was centrifuged and heated at 180°C under vacuum for 3 days. The solid-state ^{1}H MAS NMR spectrum of the dry powder clearly shows not only the endohedral water peak but also a strong peak from a protonated impurity (figure 1*b*).

An additional purification step (p2) was performed as follows: (i) the sample was washed with diethyl ether to remove ether-soluble impurities; (ii) the sample was heated to a temperature of 250°C and a pressure of approximately 2×10^{-5} mbar for 4 h to remove occluded solvent; (iii) the sample was sublimed onto the walls of a clean 6 mm outer-diameter silica tube. The sublimation was carried out by heating the sample from room temperature to 550°C at 1°C min^{-1} and then maintaining this temperature for 12 h.

The solid-state ^{1}H MAS NMR spectrum of the sample after procedures p1 and p2 is shown in figure 1*c*. The intensity of the protonated impurity peak is greatly reduced compared with that in figure 1*b*, indicating the almost complete removal of protonated impurities. The weak broad feature is attributed to protonated parts of the MAS rotor assembly and the NMR probe.

In addition to the large improvement in purity, the half-width at half-height of the endohedral proton peak is reduced from approximately 0.15 ppm in figure 1*b* to approximately 0.04 ppm in figure 1*c*. This indicates that sublimation leads to a more homogeneous and better ordered solid-state structure.

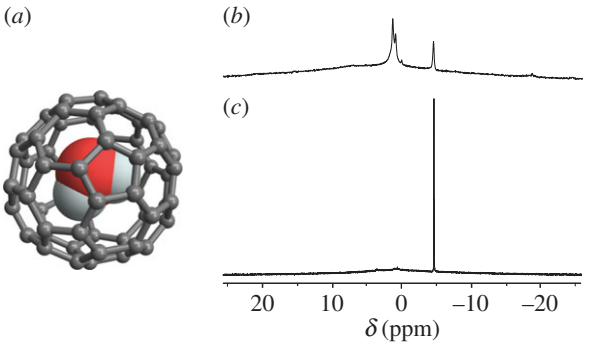

Figure 1. (*a*) The molecular structure of endohedral water fullerene, $H_2O@C_{60}$; (*b*) ^{1}H MAS NMR spectrum of $H_2O@C_{60}$ after purification method p1; and (*c*) ^{1}H MAS NMR spectrum of $H_2O@C_{60}$ after purification methods p1 and p2. The spinning frequency was 8.00 kHz in both cases and the spectra have the same vertical scale. The peak of endohedral water is at −4.7 ppm. (Online version in colour.)

All results presented below were obtained on a 2.4 mg sample of $H_2O@C_{60}$ that had undergone both procedures p1 and p2, packed in a 4 mm outer-diameter zirconia rotor.

(b) Equipment

The solid-state NMR experiments reported in this paper were performed on a Varian Infinity+ spectrometer equipped with a 9.4 T magnet, corresponding to a ^{1}H resonance frequency of 400 MHz. All experiments were performed with the sample at room temperature.

(c) Spectroscopic techniques

(i) Static proton NMR

Proton NMR spectra were obtained without sample rotation by acquiring the NMR signal induced by a 90° pulse. The proton pulse duration was 3.5 μs.

(ii) Magic-angle-spinning NMR

Proton MAS NMR spectra were obtained by rotating the sample at the 'magic angle' $\arctan\sqrt{2} \simeq 54.7°$ with respect to the static magnetic field and applying a 90° pulse. The rotation frequencies used in these experiments were between 1.00 and 5.00 kHz. All chemical shift scales are referenced to the 1.8 ppm proton peak of solid adamantane.

(iii) Double-quantum-filtered dipolar recoupling

A variety of methods are available for studying ^{1}H–^{1}H dipolar couplings in solids [15–17]. In the present work, symmetry-based dipolar recoupling was used to estimate the residual proton–proton coupling. The pulse sequence is sketched in figure 2. The sequence is performed under MAS conditions and is rotor synchronized. The dipolar recoupling is induced by using a supercycled symmetry-based sequence of the form $SR20_2^9$ [18]. Repeated $SR20_2^9$ supercycles are applied for an excitation time interval, τ_{exc}, during which double-quantum coherence builds up. A 90° phase-shifted sequence of $SR20_2^9$ supercycles is applied for the reconversion time interval, τ_{rec}, followed by a 90° pulse, which induces an NMR signal. Signals passing through double-quantum coherence are isolated by a double-quantum filter, implemented by a 16-step phase cycle.

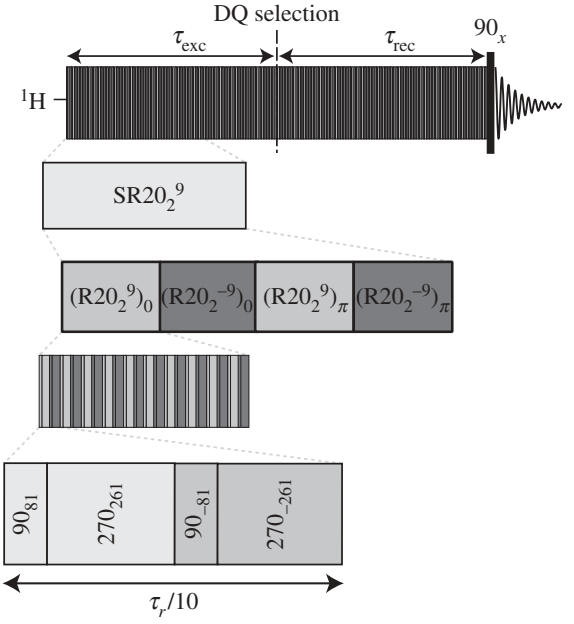

Figure 2. Double-quantum-filtered dipolar recoupling sequence used to measure residual dipolar couplings in $H_2O@C_{60}$. The supercycle SR20$_2^9$ consists of four symmetry-based recoupling cycles of the form R20$_2^{\pm 9}$, with overall phase shifts of $\{0, 0, \pi, \pi\}$. Each R20$_2^{\pm 9}$ cycle consists of 10 pairs of two-element composite pulses, with phase shifts of $\pm 9\pi/20$. The radiofrequency field strength is adjusted to match the duration of each R20$_2^{\pm 9}$ cycle with two periods of the MAS rotor. The complete pulse sequence involves a double-quantum excitation sequence of duration τ_{exc}, which converts equilibrium magnetization to double-quantum coherence. This is followed by a double-quantum reconversion sequence, which converts double-quantum coherence back to longitudinal magnetization, which is transformed into observable transverse magnetization by a $\pi/2$ pulse. Phase cycling is used to suppress NMR signals that did not pass through double-quantum coherence.

The SR20$_2^9$ supercycle consists of the following scheme [18]:

$$\mathrm{SR20_2^9} = \left[\mathrm{R20_2^9 R20_2^{-9}}\right]_0 \left[\mathrm{R20_2^{-9} R20_2^9}\right]_\pi ,$$

which combines sign alternation of the winding number with a sequence of overall phase shifts. As described in Webber *et al*. [15], this supercycle compensates second-order terms in the recoupled Hamiltonian, which is important for the measurement of small dipolar couplings, at the expense of removing the γ-encoding feature of the pure R20$_2^9$ pulse sequence. Although this reduces the maximum double-quantum efficiency, this loss is more than compensated by the increased robustness [18].

All double-quantum recoupling experiments were performed at a spinning frequency of 8.00 kHz. The double-quantum excitation interval τ_{exc} was incremented from 0 to 7.25 ms in steps of 0.25 ms. The double-quantum reconversion interval τ_{rec} was decremented by the same amount, so that the total recoupling interval $\tau_{exc} + \tau_{rec}$ was kept constant at 7.25 ms (symmetric protocol [19]). The integrated signal plotted versus τ_{exc} gives rise to the double-quantum build-up curve that is analysed to yield the value of the dipolar coupling constant.

(d) Numerical simulations

All numerical simulations were run using the SIMPSON simulation package [20].

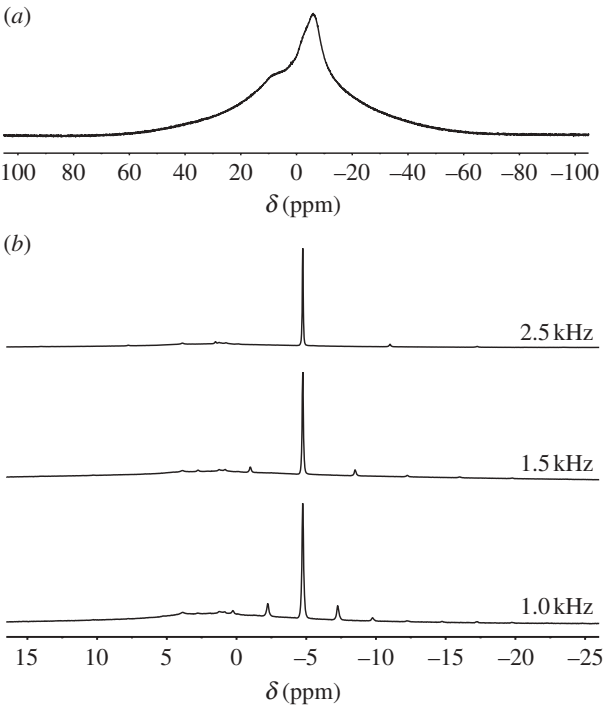

Figure 3. (*a*) Static ^{1}H spectrum of $H_2O@C_{60}$ obtained from 4196 accumulated transients. (*b*) ^{1}H MAS spectra of the same sample at the indicated spinning frequencies. The MAS spectra are derived from 256 accumulated transients.

(i) Proton magic-angle-spinning spectra

Proton MAS spectra were simulated for the experimental spinning frequency of 1.00 kHz. The powder average was simulated by using the SIMPSON crystal file *rep100* together with 10 evenly distributed γ angles. The simulations were performed for randomly oriented proton pairs with dipolar coupling and CSA interactions. Both the dipolar coupling and CSA interactions were described by uniaxial tensors, with the relative orientation of the unique principal axes described by the angle β. The angle β was varied in a series of simulations (see below).

(ii) Double-quantum-filtered dipolar recoupling simulations

The DQfDR experiment was simulated for randomly oriented pairs of dipolar-coupled protons with no CSA. The powder average was simulated by using the SIMPSON crystal file *bcr20* together with 20 evenly distributed γ angles. A grid of simulations was compiled by varying the dipolar coupling constant in the range $-600\,\text{Hz} < b/(2\pi) < -400\,\text{Hz}$ in steps of 20 Hz. The dipolar coupling was estimated by comparing the grid of simulations to the experimental data. It was verified by simulation that inclusion of a 2.9 ppm CSA interaction has no effect on the estimated dipolar coupling constant.

3. Results

(a) Static ^{1}H NMR

The static solid-state ^{1}H NMR spectrum of $H_2O@C_{60}$ displays a broad peak with a linewidth of several kHz (figure 3*a*). The lineshape is due to long-range dipole–dipole interactions and contains no useful local information.

(b) Magic-angle-spinning ^{1}H NMR

MAS NMR averages out anisotropic interactions such as dipole–dipole couplings and chemical shift anisotropies, providing well-resolved NMR peaks for solid samples, at the isotropic chemical shift frequencies. The sample rotation generates periodic spinning sidebands displaced from the isotropic chemical shifts by multiples of the spinning frequency. The amplitudes of the spinning sidebands may be analysed to obtain information on the anisotropic local nuclear spin interactions.

A set of ^{1}H MAS spectra of $H_2O@C_{60}$, obtained at three different spinning frequencies, is shown in figure 3*b*. The proton MAS spectra display a strong narrow peak at the chemical shift of −4.7 ppm, which is very close to the reported chemical shift for $H_2O@C_{60}$ in solution (−4.81 ppm [3]). Spinning sidebands are visible at low (less than 5 kHz) spinning frequencies, indicating that residual anisotropic interactions are present, but with a smaller magnitude than those observed at cryogenic temperatures [4].

Two kinds of spin interactions can contribute to the spinning sideband pattern observed at low spinning frequency: through-space dipolar coupling and CSA. The contributions of these two different interactions may not be disentangled without additional spectroscopic data.

(c) Double-quantum dipolar recoupling

The effect of dipole–dipole coupling interactions may be distinguished from CSA interactions by using selective dipolar recoupling methods, for example, those based on the rotational symmetry of the spin interactions [19,21]. Symmetry-based double-quantum recoupling was used previously on a highly asymmetric open-cage form of the endofullerene $H_2@C_{60}$ in order to investigate the anisotropy of the H_2 rotation [14]. Since the anisotropic interactions in $H_2O@C_{60}$ are much smaller than those encountered in [14], a modified double-quantum procedure was used for the current work, based on the robust error-compensated supercycle $SR20_2^9$, as described in §2.

The double-quantum recoupling procedure results in a plot of peak intensity versus the double-quantum excitation time τ_{exc}. The results for $H_2O@C_{60}$ are shown in figure 4, where the filled circles represent the experimental amplitudes of the water proton peak. The double-quantum-filtered spectral amplitude is at a maximum when the excitation and reconversion intervals are equal ($\tau_{exc} = \tau_{rec} = 7.25$ ms). The dependence of the spectral amplitude on the excitation and reconversion times away from this maximum may be analysed to estimate the dipole–dipole coupling constant.

The value of the dipolar coupling constant is retrieved by comparing the experimental build-up curve with numerical simulations. The signal areas of the simulated spectra as a function of τ_{exc} are reported in figure 4 as solid curves. The best match between simulation and experiments occurs for a dipolar coupling constant $|b/(2\pi)| = 500$ Hz. The confidence limits on this dipolar coupling constant are approximately ±10 Hz.

(d) Estimation of chemical shift anisotropy

A numerical simulation of the NMR spectrum generated by randomly oriented proton pairs at a spinning frequency of 1.00 kHz, and with a dipolar coupling $b/(2\pi) = -500$ Hz, is shown in figure 5*a* (second from the bottom). The simulated spinning sidebands have a significantly smaller intensity than in the experimental spectrum (figure 5*a*, grey spectrum at the bottom). The poor match between simulation and experiment indicates that the dipole–dipole coupling, as estimated by the double-quantum recoupling experiment, cannot be solely responsible for the MAS spinning sideband intensities. A CSA interaction must contribute as well.

The magnitude and orientation of the CSA were estimated by comparing ^{1}H MAS spectra with simulations, at a spinning frequency of 1.00 kHz (figure 5). For simplicity, the simulations assumed randomly oriented pairs of protons with uniaxial dipolar and chemical shift tensors. The

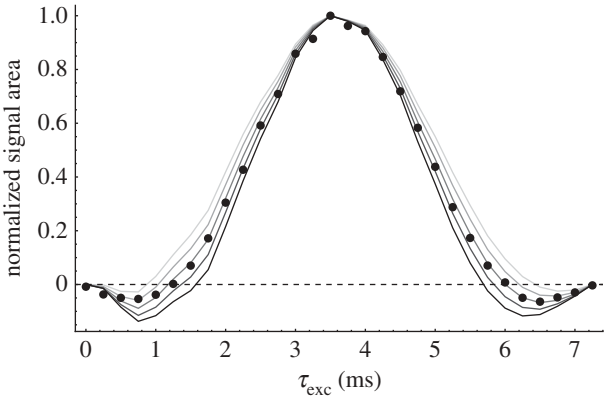

Figure 4. Double-quantum-filtered signal areas as a function of the recoupling interval τ_{exc} obtained in a symmetric double-quantum recoupling procedure, using the pulse sequence $SR20_2^9$ at a spinning frequency of 1.00 kHz (figure 2). Circles represent the experimental values. Solid curves from grey to black represent numerical simulations for dipolar coupling constants $|b/(2\pi)| = 460, 480, 500, 520$ and 540 Hz. The data were normalized to 1 at the maximum recoupling efficiency.

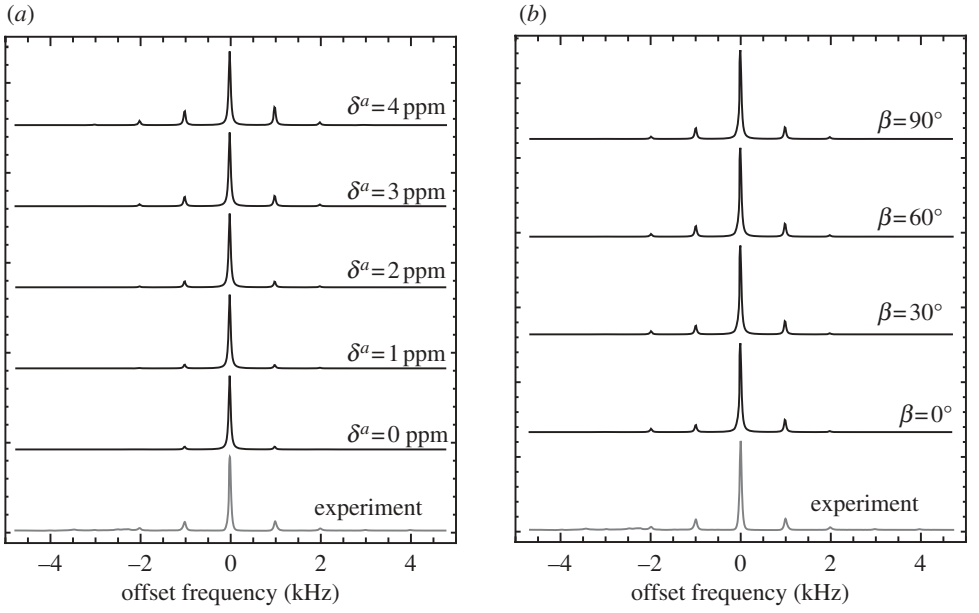

Figure 5. Simulated ^{1}H MAS spectra (black lines) of randomly oriented proton pairs at a spinning frequency of 1.00 kHz, with a dipolar coupling constant $b/(2\pi) = -500$ Hz and an additional CSA interaction. The CSA tensor is assumed to be uniaxial, with magnitude $\delta^a = \delta_{zz} - \delta_{iso}$, and with the unique axis at an angle β with respect to the ^{1}H–^{1}H dipole–dipole coupling tensor. (*a*) Simulations for $\beta = 90^\circ$ at the indicated values of δ^a; and (*b*) simulations for $\delta^a = 3.1$ ppm at the indicated values of β. The experimental spectra for $H_2O@C_{60}$ are shown at the bottom of each panel.

value of the dipolar coupling constant was set to −500 Hz, as determined by the double-quantum recoupling experiment. The motionally averaged chemical shift tensors of the two protons were assumed to be identical and uniaxial. The unique principal axis of the CSA tensor was assumed to subtend an angle β with the unique principal axis of the dipole–dipole coupling tensor. The CSA δ^a (defined as $\delta^a = \delta_{zz} - \delta_{iso}$, where δ_{zz} is the principal axis of the chemical shift tensor that is most distant from the isotropic value δ_{iso}) and the angle β were varied independently in a set of simulations and compared with the experimental spectrum.

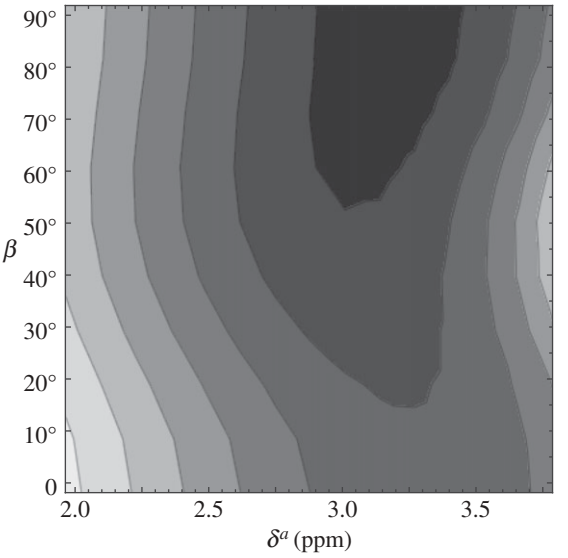

Figure 6. Contour map of the χ^2 statistic equation (3.1) plotted versus the CSA δ^a and the angle β between the principal axes of the chemical shift and dipole–dipole interactions. Low values of χ^2 are indicated by dark shading. The darkest area represents the 68% confidence region. This plot shows that the ^{1}H CSA tensor is most likely to be perpendicular to the ^{1}H–^{1}H dipolar coupling tensor.

The best match between experiment and simulations was obtained for $|\delta^a| = 3.1$ ppm and $\beta = 90^\circ$. The simulated spectrum is insensitive to the signs of both the CSA δ^a and the dipole–dipole coupling in the best-fitted region, so these signs cannot be determined unambiguously. The confidence limits on $\{\delta^a, \beta\}$ were estimated by a χ^2 analysis [22] using

$$\chi^2(\delta^a, \beta) = \sum_{i=-2}^{2} (I_i^{\mathrm{S}}(\delta^a, \beta) - I_i^{\mathrm{E}})^2, \tag{3.1}$$

where I_i^{E} indicates the area of the ith-order sideband in the experimental spectrum and $I_i^{\mathrm{S}}(\delta^a, \beta)$ is the area of the ith-order sideband in the spectrum simulated for given values of the parameters δ^a and β. A plot of χ^2 against $\{\delta^a, \beta\}$ is shown in figure 6.

Rough 68% confidence limits on the parameters were estimated from the bounds of the region. The estimated CSA parameters, and their confidence limits, are $|\delta^a| = 3.1 \pm 0.3$ ppm and $\beta = 90^\circ \pm 40^\circ$. This indicates that the unique principal axis of the CSA tensor is approximately perpendicular to the dipole–dipole coupling tensor.

(e) Discussion

The double-quantum ^{1}H dipolar recoupling experiment finds clear evidence of a ^{1}H–^{1}H dipolar coupling interaction in $H_2O@C_{60}$ at room temperature, with magnitude $|b/(2\pi)| = 500 \pm 10$ Hz. Analysis of the MAS ^{1}H spectrum indicates the simultaneous presence of a ^{1}H CSA interaction, of magnitude 3.1 ppm, and with a unique principal axis that is perpendicular to that of the dipole–dipole coupling tensor.

What is the physical interpretation of these results?

Three competing physical models are sketched in figure 7. Model (*a*) represents a situation in which the enclosing cage retains its icosahedral symmetry. A local electric field, with origin outside the cage, partially orients the endohedral water molecules. This partial orientation leads to a residual dipole–dipole coupling, and also a residual CSA interaction, since the ^{1}H CSA associated with the water molecule itself is not averaged to zero. In model (*b*), the distribution

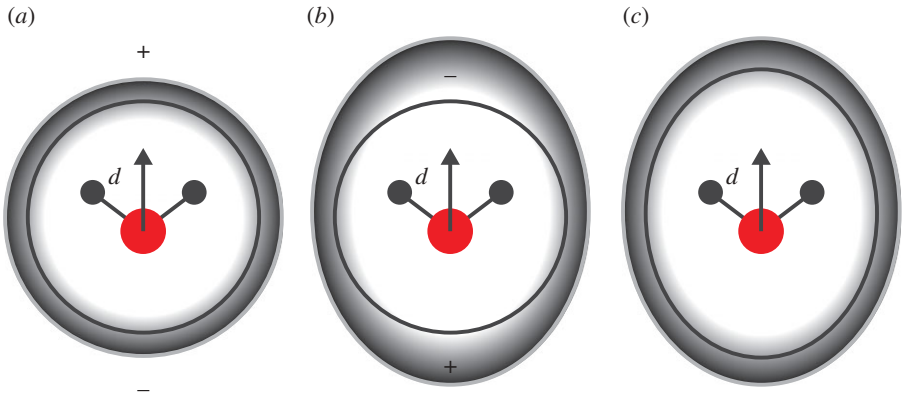

Figure 7. Models of water–cage interactions. (*a*) The water electric dipoles are partially oriented by an external electric field, but without distortion of the cage. (*b*) The electric dipole moment of water induces a change in the electronic distribution of the cage, but without influencing its geometry. (*c*) The water molecule distorts the shape of the cage. (Online version in colour.)

of delocalized cage electrons is perturbed by the presence of the water electric dipole, but the geometry of the cage remains unchanged. The anisotropic cage environment generates an anisotropic magnetic field, and hence a CSA interaction, for the endohedral water protons. In model (*c*), the perturbation of the cage by the endohedral water is not electronic in nature, but structural. A residual CSA for the endohedral water is caused by the electrons of the anisotropic cage. Combinations of these mechanisms are also feasible.

The geometry of a water molecule constrains the proton–proton vector to be perpendicular to the electric dipole moment. If the CSA is averaged by molecular motion around the electric dipole moment, then all mechanisms (*a*), (*b*) and (*c*) are consistent with the experimental observation $\beta \simeq 90^\circ$.

Mechanism (*a*) leads to a predictable ratio of the motionally averaged dipole–dipole coupling and the CSA, since both are caused by partial orientation of the water electric dipole with respect to an external axis. The motionally averaged proton dipole–dipole coupling of a water molecule with its electric dipole moment partially aligned with the external electric field is

$$\langle b \rangle = b_{\mathrm{HH}} P_2\left(\cos \beta_{\mathrm{PD}}^{\mathrm{HH}}\right) S^2, \tag{3.2}$$

while the motionally averaged proton CSA is

$$\left\langle \delta^a \right\rangle = \delta_{\mathrm{intra}}^a P_2\left(\cos \beta_{\mathrm{PD}}^{\mathrm{CSA}}\right) S^2, \tag{3.3}$$

where $b_{\mathrm{HH}} = -(\mu_0/4\pi)\gamma_{\mathrm{H}}^2 \hbar r_{\mathrm{HH}}^{-3}$ is the dipolar constant of two protons separated by a distance r_{HH}, $\delta_{\mathrm{intra}}^a$ is the CSA for an immobilized water molecule, caused by intramolecular local fields, $\beta_{\mathrm{PD}}^{\mathrm{HH}}$ is the angle between the ^{1}H–^{1}H vector and the electric dipole moment, and $\beta_{\mathrm{PD}}^{\mathrm{CSA}}$ is the angle between the major principal axis of the ^{1}H chemical shift tensor and the electric dipole moment. Here S^2 is the second-rank order parameter, given by

$$S^2 = \langle P_2(\cos \beta_{\mathrm{DE}}) \rangle ,$$

where β_{DE} is the angle between the electric dipole moment of an individual water molecule and a fixed external axis. The second-rank Legendre polynomial is denoted as $P_2(x) = \frac{1}{2}(3x^2 - 1)$.

The equilibrium geometry of H_2O is given by $R_{\mathrm{OH}} = 0.958$ Å and $\angle_{\mathrm{HOH}} = 104.5^\circ$ [22] so that $r = 1.515$ Å and $b_{\mathrm{HH}}/(2\pi) = -34.5$ kHz. The geometry of water is such that the proton–proton vector is perpendicular to the electric dipole moment ($\beta_{\mathrm{PD}}^{\mathrm{HH}} = \pi/2$). From the measured value $|b| = 500$ Hz, we obtain an estimated second-rank order parameter of $S^2 = 0.029$.

The intramolecular contribution to the CSA may be estimated from solid-state NMR measurements of immobilized water molecules in calcium sulfate dihydrate (gypsum), providing $\delta^a_{\mathrm{intra}} = 3.4\,\mathrm{ppm}$ [23]. If the CSA principal axis is assumed to be along the OH bond, then the CSA orientation angle is estimated to be $\beta_{\mathrm{PD}}^{\mathrm{CSA}} \simeq \frac{1}{2} \times 104.5^\circ \simeq 52.3^\circ$. These pieces of information may be combined to obtain a theoretical value of the motionally averaged CSA under model (*a*): $\langle \delta^a \rangle (a) \simeq 0.024\,\mathrm{ppm}$. This is much smaller than the experimental estimate $\delta^a = 3.1\,\mathrm{ppm}$. We conclude that model (*a*) is not tenable.

The observed proton CSA for $H_2O@C_{60}$ is therefore unlikely to be associated with the water molecule itself, but must be mainly generated by the cage. This implies that the electronic distribution of the cage is distorted (mechanism (*b*)) or that the geometry of the cage is distorted (mechanism (*c*)), or a combination of the two.

4. Conclusion

This work investigated the magnitude and relative orientation of anisotropic spin interactions in $H_2O@C_{60}$ at room temperature by means of solid-state NMR spectroscopy and numerical simulations. We obtained evidence for a significant residual ^{1}H CSA as well as a residual proton–proton dipolar coupling. The presence of these spin interactions at room temperature could be due either to a partial alignment of the water molecules or to a distortion of the cage's geometry or electronic structure. Our data exclude the hypothesis of partial water alignment within unperturbed fullerene cages, supporting models in which the water molecule leads to a geometrical distortion of the surrounding cage, or a polarization of cage electrons.

In principle, quantum calculations could determine the electronic configuration and geometry of the $H_2O@C_{60}$ complex. Furthermore, distortion of the cage breaks the icosahedral symmetry and removes the equivalence of the ^{13}C sites. High-resolution ^{13}C NMR spectra may resolve ^{13}C chemical shifts due to non-equivalent carbons in cages of reduced symmetry. Studies of this kind are in progress.

Acknowledgements. M.C. acknowledges a University Research Fellowship from the Royal Society (UK); we also thank E. Carignani (Pisa, Italy) for experimental help.

Funding statement. We thank EPSRC (UK) and The National Science Foundation (USA) for funds.

References

1. Rubin Y. 1999 Ring opening reactions of fullerenes: designed approaches to endohedral metal complexes. *Top. Curr. Chem.* **199**, 67–91. (doi:10.1007/3-540-68117-5_2)
2. Komatsu K, Murata M, Murata Y. 2005 Encapsulation of molecular hydrogen in fullerene C_{60} by organic synthesis. *Science* **307**, 238–240. (doi:10.1126/science.1106185)
3. Kurotobi K, Murata Y. 2011 A single molecule of water encapsulated in fullerene C_{60}. *Science* **333**, 613–616. (doi:10.1126/science.1206376)
4. Beduz C *et al.* 2012 Quantum rotation of *ortho* and *para*-water encapsulated in a fullerene cage. *Proc. Natl Acad. Sci. USA* **109**, 12 894–12 898. (doi:10.1073/pnas.1210790109)
5. Carravetta M, Johannessen OG, Levitt MH, Heinmaa I, Stern R, Samoson A, Horsewill AJ, Murata Y, Komatsu K. 2006 Cryogenic NMR spectroscopy of endohedral hydrogen–fullerene complexes. *J. Chem. Phys.* **124**, 104507. (doi:10.1063/1.2174012)
6. Carravetta M *et al.* 2007 Solid-state NMR of endohedral hydrogen–fullerene complexes. *Phys. Chem. Chem. Phys.* **9**, 4879–4894. (doi:10.1039/b707075f)
7. Mamone S *et al.* 2009 Rotor in a cage: infrared spectroscopy of an endohedral hydrogen–fullerene complex. *J. Chem. Phys.* **130**, 081103. (doi:10.1063/1.3080163)
8. Horsewill AJ *et al.* 2010 Inelastic neutron scattering of a quantum translator–rotator encapsulated in a closed fullerene cage: isotope effects and translation–rotation coupling in $H_2@C_{60}$ and $HD@C_{60}$. *Phys. Rev. B.* **82**, 081410. (doi:10.1103/PhysRevB.82.081410)
9. Mamone S, Chen JY-C, Bhattacharyya R, Levitt MH, Lawler RG, Horsewill AJ, Rõõm T, Bačić Z, Turro NJ. 2011 Theory and spectroscopy of an incarcerated quantum rotor: the infrared spectroscopy, inelastic neutron scattering and nuclear magnetic resonance of $H_2@C_{60}$ at cryogenic temperature. *Coord. Chem. Rev.* **255**, 938–948. (doi:10.1016/j.ccr.2010.12.029)

10. Ge M *et al.* 2011 Interaction potential and infrared absorption of endohedral H_2 in C_{60}. *J. Chem. Phys.* **134**, 054507. (doi:10.1063/1.3535598)
11. Ge M *et al.* 2011 Infrared spectroscopy of endohedral HD and D_2 in C_{60}. *J. Chem. Phys* **135**, 114511. (doi:10.1063/1.3637948)
12. Xu M, Sebastianelli F, Bačić Z, Lawler R, Turro NJ. 2008 H_2, HD, and D_2 inside C_{60}: coupled translation–rotation eigenstates of the endohedral molecules from quantum five-dimensional calculations. *J. Chem. Phys.* **129**, 064313. (doi:10.1063/1.2967858)
13. Xu M, Sebastianelli F, Gibbons BR, Bačić Z, Lawler R, Turro NJ. 2009 Coupled translation–rotation eigenstates of H_2 in C_{60} and C_{70} on the spectroscopically optimized interaction potential: effects of cage anisotropy on the energy level structure and assignments. *J. Chem. Phys.* **130**, 224306. (doi:10.1063/1.3152574)
14. Levitt MH. 2002 Symmetry-based pulse sequences in magic-angle spinning solid-state NMR. In *Encyclopedia of Nuclear Magnetic Resonance*, vol. 9 (supplementary volume), *Advances in NMR* (eds DM Grant, RK Harris), pp. 165–195. Chichester, UK: John Wiley & Sons.
15. Webber AL *et al.* 2010 Complete ^{1}H resonance assignment of β-maltose from ^{1}H-^{1}H DQ-SQ CRAMPS and ^{1}H (DQ-DUMBO)–^{13}C SQ refocused INEPT 2D solid-state NMR spectra and first principles GIPAW calculations. *Phys. Chem. Chem. Phys.* **12**, 6970–6983. (doi:10.1039/c001290d)
16. Brown SP, Spiess HW. 2001 Advanced solid-state NMR methods for the elucidation of structure and dynamics of molecular, macromolecular, and supramolecular systems. *Chem. Rev.* **101**, 4125–4155. (doi:10.1021/cr990132e)
17. Feike M, Demco DE, Graf R, Gottwald J, Hafner S, Spiess HW. 1996 Broadband multiple-quantum NMR spectroscopy. *J. Magn. Reson. A* **122**, 214–221. (doi:10.1006/jmra.1996.0197)
18. Kristiansen PE, Carravetta M, Lai WC, Levitt MH. 2004 A robust pulse sequence for the determination of small homonuclear dipolar couplings in magic-angle spinning NMR. *Chem. Phys. Lett.* **390**, 1–7. (doi:10.1016/j.cplett.2004.03.075)
19. Carravetta M, Eden M, Brinkmann A, Zhao X, Levitt MH. 2000 Symmetry principles for the design of radiofrequency pulse sequences in the nuclear magnetic resonance of rotating solids. *Chem. Phys. Lett.* **321**, 205–215. (doi:10.1016/S0009-2614(00)00340-7)
20. Bak M, Rasmussen JT, Nielsen NC. 2000 SIMPSON: a general simulation program for solid-state NMR spectroscopy. *J. Magn. Reson.* **147**, 296–330. (doi:10.1006/jmre.2000.2179)
21. Levitt MH. 2008 Symmetry in the design of NMR multiple-pulse sequences. *J. Chem. Phys.* **128**, 052205. (doi:10.1063/1.2831927)
22. Bunker PR, Jenesen P. 2006 *Molecular symmetry and spectroscopy*. Ottawa, Canada: NRC Research Press.
23. McKnett CL, Dybowski CR, Vaughan RW. 1975 High resolution proton NMR of gypsum, $CaSO_4 \cdot 2H_2O$. *J. Chem. Phys.* **63**, 4578–4581. (doi:10.1063/1.431266)